Modulation of the slow/common gating of CLC channels by intracellular cadmium

Yawei Yu,[1,2] Ming-Feng Tsai,[3] Wei-Ping Yu,[1,2] and Tsung-Yu Chen[1,2]

[1]Center for Neuroscience and [2]Department of Neurology, University of California, Davis, Davis, CA 95618
[3]Department of Biochemistry, Howard Hughes Medical Institute, Brandeis University, Waltham, MA 02453

Members of the CLC family of Cl^- channels and transporters are homodimeric integral membrane proteins. Two gating mechanisms control the opening and closing of Cl^- channels in this family: fast gating, which regulates opening and closing of the individual pores in each subunit, and slow (or common) gating, which simultaneously controls gating of both subunits. Here, we found that intracellularly applied Cd^{2+} reduces the current of CLC-0 because of its inhibition on the slow gating. We identified CLC-0 residues C229 and H231, located at the intracellular end of the transmembrane domain near the dimer interface, as the Cd^{2+}-coordinating residues. The inhibition of the current of CLC-0 by Cd^{2+} was greatly enhanced by mutation of I225W and V490W at the dimer interface. Biochemical experiments revealed that formation of a disulfide bond within this Cd^{2+}-binding site is also affected by mutation of I225W and V490W, indicating that these two mutations alter the structure of the Cd^{2+}-binding site. Kinetic studies showed that Cd^{2+} inhibition appears to be state dependent, suggesting that structural rearrangements may occur in the CLC dimer interface during Cd^{2+} modulation. Mutations of I290 and I556 of CLC-1, which correspond to I225 and V490 of CLC-0, respectively, have been shown previously to cause malfunction of CLC-1 Cl^- channel by altering the common gating. Our experimental results suggest that mutations of the corresponding residues in CLC-0 change the subunit interaction and alter the slow gating of CLC-0. The effect of these mutations on modulations of slow gating of CLC channels by intracellular Cd^{2+} likely depends on their alteration of subunit interactions.

The Journal of General Physiology

INTRODUCTION

Members of the CLC Cl^- channel/transporter family participate in a wide spectrum of biological processes from extreme acid resistance in enteric bacteria to lysosomal acidification and membrane voltage regulation in mammalian cells (Jentsch, 2008; Jentsch et al., 2005; Stauber et al., 2012). These CLC proteins contain two identical subunits (Middleton et al., 1994, 1996; Ludewig et al., 1996), each forming a Cl^--transport pathway (Dutzler et al., 2002, 2003). In eukaryotic CLC Cl^- channels, such as CLC-0 and CLC-1, the individual anion-transport pathways (or pores) are gated by the negatively charged side chain of a glutamate residue (Dutzler et al., 2003). The swing of this glutamate side chain is believed to be responsible for the "fast gating" operating in the time range of milliseconds. There is a second gating mechanism called "slow gating" (for CLC-0) or "common gating" (for CLC-1), which controls the opening and closing of both pores simultaneously with a slower kinetics (Chen, 2005; Miller, 1982; Miller and White, 1984). Although recent work has identified certain molecular determinants for the slow/common gating of CLC channels (Bennetts and Parker, 2013), the exact mechanism of this gating process is not well understood.

It has been suggested that interactions between the two CLC subunits are involved in the slow/common gating processes (Estévez and Jentsch, 2002; Bykova et al., 2006). Crystal structures of the *Escherichia coli* CLC (CLC-ec1) and a eukaryotic CLC transporter CmCLC show extensive helix packing in the subunit interface (Dutzler et al., 2002; Feng et al., 2010; Robertson et al., 2010). At this flat, nonpolar interface, hydrophobic residues such as valine, leucine, and isoleucine form most of the cross-subunit contacts (Dutzler et al., 2002; Robertson et al., 2010). Replacing two isoleucine residues, I201 and I422, at the dimer interface of CLC-ec1 (see Fig. 1 for the locations of these two residues) with tryptophan disrupts the dimeric architecture, and the I201W/I422W double mutant of CLC-ec1 exists as a monomer (Robertson et al., 2010). Coincidentally, previous work has also demonstrated that mutations of I290 and I556 of CLC-1 (which correspond to I201 and I422, respectively, in CLC-ec1) alter the common gating (Pusch et al., 1995; Kubisch et al., 1998; Saviane et al., 1999). Collectively, these results suggest that molecular

Correspondence to Tsung-Yu Chen: tycchen@ucdavis.edu

Abbreviations used in this paper: FRET, fluorescent resonant energy transfer; HEK, human embryonic kidney; MTSES, 2-sulfonatoethyl MTS; MTSET, 2-(trimethylammonium)ethyl MTS.

The Rockefeller University Press $30.00
J. Gen. Physiol. Vol. 146 No. 6 495–508
www.jgp.org/cgi/doi/10.1085/jgp.201511413

events occurring in the CLC dimer interface contribute to slow/common gating.

The research in our laboratory has revealed previously that extracellular zinc ions (Zn^{2+}) inhibit CLC-0 by facilitating the closure of slow gate, although the Zn^{2+}-binding site for this effect is not known (Chen, 1998). In the present study, we find that intracellular transition metal cations (such as Cd^{2+}) also inhibit the slow gating in WT CLC-0. We have identified that the Cd^{2+}-binding site responsible for this inhibition effect in CLC-0 is formed by C229 and H231 located at the dimer interface near the intracellular end of the transmembrane domain (Fig. 1). Interestingly, the Cd^{2+} inhibition potency in CLC-0 is drastically increased by I225W/V490W mutations, corresponding to the dimer interface mutations of I201W/I422W in CLC-ec1. In addition, formation of a disulfide bond between introduced cysteine residues in this binding site is also affected by mutations of I225W and V490W. These results show that a structural change of the Cd^{2+}-binding site, as reported by the alterations of Cd^{2+} modification and disulfide-bond formation, is induced by the dimer interface mutations, which also alter CLC channel's slow/common gating. These results thus suggest that a structural rearrangement at the dimer interface near the intracellular Cd^{2+}-binding site is likely involved in the slow/common gating of CLC channels.

MATERIALS AND METHODS

Chemicals

MTS reagents were purchased from Toronto Research Chemicals. Stock solutions of 0.3 M MTS reagents were made in distilled water and stored at −80°C. The working solutions with required concentrations of MTS reagents were made immediately before use from the stock solution placed on ice, and were discarded if not used within 5 min. Cadmium chloride ($CdCl_2$), HEPES, EGTA, and various salts for electrophysiological recordings were from Sigma-Aldrich and Thermo Fisher Scientific.

Mutagenesis and channel expression

The CLC-0 and CLC-1 cDNAs used for electrophysiological recordings were constructed in the pcDNA3 vector without any genetic tags of fluorescent proteins. For the constructs used in biochemical experiments, a "Flag" epitope was added to the N terminus (after the first methionine) of different CLC-0 constructs subcloned in the pcDNA3 vector. Mutations were made using the QuikChange site-directed mutagenesis kit (Agilent Technologies) and were confirmed by commercial DNA sequencing services. In the fluorescent resonant energy transfer (FRET) study used to evaluate the interaction of two channel subunits (Fig. 3), the C-terminal cytoplasmic domain of CLC-0 was removed after Ser530 to make a fair comparison with CLC-ec1 because the latter lacks a cytoplasmic domain. This C terminus–truncated mutant of CLC-0, referred to as CLC0-TM, has been described previously (Bykova et al., 2006). It was constructed in the pEGFP-N3 vector, and the C terminus of the CLC0-TM sequence was tagged by a Gly-Ser linker followed by the sequence of cerulean or eYFP. The I225W/V490W mutations of CLC-0 (corresponding to I201W/I422W mutations in CLC-ec1) were made in these two CLC0-TM constructs, and were used in the FRET study. The CNG channel used as the negative control in the FRET experiment was provided by W.N. Zagotta (University of Washington, Seattle, WA), and fluorescent proteins were also tagged to the C terminus of the CNG channel.

All experiments on WT CLC-0 and its mutants were conducted in human embryonic kidney (HEK)293 cells, whereas experiments on WT and mutant CLC-1 were conducted in tsA201 cells. Transfections of cDNA into HEK293 cells or tsA201 cells followed a procedure described previously (Lin and Chen, 2003; Zhang et al., 2006, 2010; Zhang and Chen, 2009), using the lipofectamine transfection kit (Life Technologies). Experiments were performed 1–3 d after transfections.

Electrophysiological recordings

Constructs of WT or mutant CLC channels were cotransfected with the cDNA of the green fluorescent protein (GFP). The green fluorescence was visualized via an inverted microscope (DM IRB; Leica) equipped with a GFP filter (Chroma Technology Corp.). Macroscopic currents from excised inside-out membrane patches of the transfected cells were recorded according to methods described previously (Lin and Chen, 2003; Zhang et al., 2006, 2010;

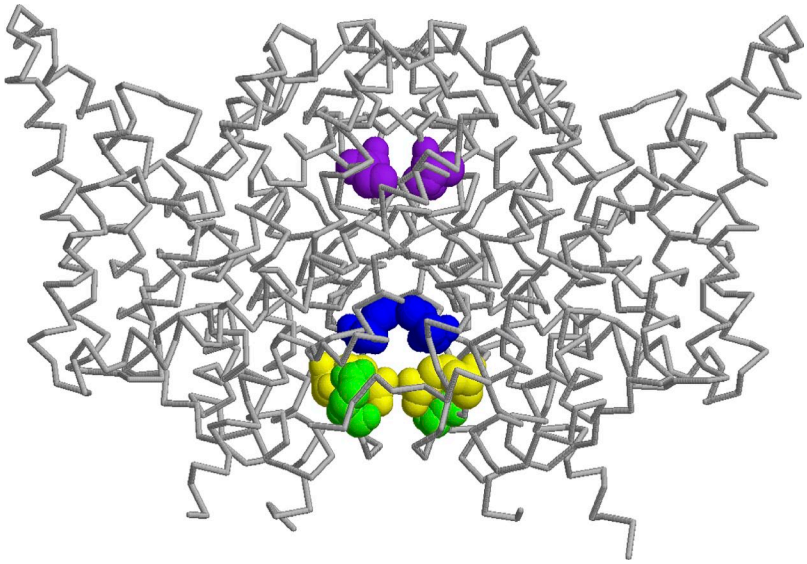

Figure 1. Crystal structure of CLC-ec1 as a guiding roadmap for examining the transmembrane domains of CLC-0 and CLC-1. The residues R205 (yellow) and Q207 (green) of CLC-ec1 correspond to C229 and H231 of CLC-0, or S294 and Y296 of CLC-1, respectively. Residues I201 (blue) and I422 (purple) are also depicted, which correspond to I225 and V490 of CLC-0, or I290 and I556 of CLC-1, respectively. The double mutations I201W/I422W in CLC-ec1 disrupted the dimeric interaction in this *E. coli* CLC and generated functional monomeric CLC-ec1 proteins (Robertson et al., 2010).

Zhang and Chen, 2009). Both Cd^{2+} and Zn^{2+} (not depicted) can inhibit WT CLC-0 from the intracellular side with roughly similar potency. However, Zn^{2+} inhibition on the I225W/V490W mutant has a slower off-rate compared with that of the Cd^{2+} inhibition. Thus, for technical convenience, we focused on the experiments using Cd^{2+}. All electrophysiological experiments were conducted using an amplifier (Axopatch 200B; Molecular Devices), and the recording traces were digitally filtered at 5 kHz, and digitized at 10 kHz using a Digidata 1440 digitizing board and pClamp10 software (Molecular Devices). The recording pipettes were fabricated from borosilicate glass capillaries (World Precision Instruments) using the pp830 pipette puller (Narishige International, Inc.). The electrodes normally had a resistance of ~1–3 MΩ when filled with the pipette (extracellular) solution containing (mM): 130 NaCl, 5 $MgCl_2$, 10 HEPES, and 1 EGTA, pH 7.4. The bath (intracellular) solution was the same as the pipette solution except that EGTA was not included in the solution containing Cd^{2+}. Because the two gating mechanisms in WT CLC-0 operate in very different time scales (Miller, 1982; Miller and White, 1984; Maduke et al., 2000; Chen, 2005), a voltage protocol containing multiple short voltage steps was used to construct the voltage-dependent activation curve (which reflects the fast-gate P_o-V curve): a prepulse at 60 mV was given before the test voltage was clamped from 60 to −160 mV for 100 ms in −20-mV voltage steps, followed by a tail voltage pulse at −100 mV. The voltage-dependent fast-gate activation curve was constructed by normalizing the initial tail current after various test voltages to that after the most depolarized test voltage. For the hyperpolarization-activated mutants such as the I225W/V490W double mutant and the mutants constructed in the I225W/V490W background, the voltage protocol included a test voltage pulse from 60 to −160 mV for 40 ms in −10-mV steps followed by a −100-mV tail pulse. The P/4 leak subtraction routine was applied to the recordings of the hyperpolarization-activated mutants because no current was detected from these mutants at the membrane voltage >0 mV.

The kinetics of the two gating mechanisms of CLC-1 (fast gating and common gating) only differs by severalfold. Separating these two gating mechanisms normally relies on two voltage protocols (referred to as protocol A and protocol B; Accardi and Pusch, 2000; Duffield et al., 2003; Bennetts et al., 2005; Tseng et al., 2007). Protocol A was used to assess the overall open probability (P_o) of CLC-1: the product of the open probability of the fast gate (P_o^f) and that of the common gate (P_o^c). In brief, the membrane voltage was clamped at 0 mV and was first stepped to various test voltages from 120 to −120 mV in −20-mV steps for 200 ms before the tail voltage step at −100 mV for 100 ms. The tail current at −100 mV was fitted to a double exponential function, and the P_o was calculated by normalizing the value of the initial tail current to the maximal initial tail current obtained after the most positive test voltage. Protocol B is basically the same as protocol A except that a short (400-µs) but very positive (170-mV) pulse was inserted before the tail voltage step to completely open the fast gate. In this case, the normalized tail current represents P_o^c at the preceding test voltage, and P_o^f can be calculated by dividing P_o by P_o^c.

In experiments where continuous monitoring of the channel current was required, the membrane potential was clamped at 0 mV. For the depolarization-activated channels (such as WT CLC-0, C212S, and CLC-1), a voltage pulse of 60 mV for 100–200 ms followed by a negative voltage of −100 mV for 100–300 ms was given every 2 s. For the hyperpolarization-activated mutants, the 60-mV voltage step of this pulse protocol was omitted. The steady-state current at the end of the negative voltage step was measured to monitor the various effects from Cd^{2+} modulation or from modification by MTS reagents. Solution exchange was achieved using a solution exchanger (SF-77; Warner Instruments). Various concentrations of Cd^{2+} or MTS reagents were applied to the intracellular side of the excised inside-out membrane patches.

Examining the kinetics of Cd^{2+} inhibition on the I225W/V490W mutant is challenging because monitoring the channel current requires negative voltage pulses that relieve the binding of the Cd^{2+}. We therefore designed a two-pulse protocol for studying the kinetics of Cd^{2+} inhibition. To evaluate the inhibition rate of intracellular Cd^{2+}, a −100-mV voltage pulse for 50 ms was first given to obtain the initial current in the absence of Cd^{2+}, followed by exposing the patch to various concentrations of Cd^{2+} at 0, −40, or −80 mV for various periods of time before the same pulse was given again to measure the remaining current (Fig. 12 A). Combining multiple traces from experiments using this two-pulse protocol generates the time course of the Cd^{2+} inhibition (Fig. 12 B). To measure the recovery rate of Cd^{2+} inhibition, a 50-ms voltage pulse to −100 mV was given to obtain the control current, followed by exposing the patch to 300 µM Cd^{2+} for 2 s. Cd^{2+} was then washed out for various amounts of time at 0, −40, or −80 mV before a second voltage pulse was given to assess the current. The current recorded from the second pulse was normalized to the control current before Cd^{2+} inhibition.

All solution exchanges were achieved by using a solution exchanger (SF-77; Warner Instruments). The time for the electrode tip to cross the border of two laminar flows from the solution delivery pipe of the exchanger is only 2 ms (Zhang and Chen, 2009). Including the dead time of triggering the motor that moves the solution delivery pipes, the solution exchange is usually completed within 20–50 ms.

FRET experiments and analyses

Experimental methods for the FRET experiments have been described previously (Bykova et al., 2006). In brief, an inverted fluorescence microscope (IX-81; Olympus) equipped with a 100-W mercury lamp was used for imaging. The intensity of the excitation light was controlled by a set of neutral density filters installed in a filter wheel, and the duration of light exposure was controlled by a computer-driven mechanical shutter (IX2-SHA; Olympus) using Metamorph software (Molecular Devices). The cell images and the images of their spectra were recorded by a CCD camera (128B; Roper Scientific). For FRET measurements, two filter cubes (Chroma Technology Corp.) were used: Cube I (excitation filter D436/20 and dichroic mirror 455dclp) was used to excite cerulean; Cube II (excitation filter HQ500/20 and dichroic mirror Q515lp) was used to excite eYFP. No emission filter was used in these cubes. Autofluorescence from untransfected cells was negligible in all experiments.

Fluorescence imaging and analysis were performed using the Metamorph software (Molecular Devices). The experiments were achieved by user-designed journals that initiated automatic collection of a bright field cell image, the fluorescence cell images (taken with 50 ms of light exposure), and finally the spectral images (800 ms of light exposure). Spectral images were generated from the fluorescence signal on the cell by passing the imaging through a slit of a spectrograph (Acton SpectraPro 2150i; Princeton Instruments; Fig. 3 A); the same slit position was applied to both the spectrum from cerulean excitation and the spectrum from eYFP excitation. Fluorescence signals from the truncated WT CLC-0 and the truncated I225W/V490W mutant can be clearly identified at the membrane (Fig. 3 A). Therefore, the edge of the spectra corresponding to the membrane fluorescent signal was used for FRET analysis. Background light spectra, collected from the blank region of the same image, were subtracted from the cerulean and the eYFP spectral signals.

FRET involves a nonradiative transfer of light-induced excitation from one fluorophore (donor) to another (acceptor) when the donor and acceptor are located within a distance of <100 Å

(Miyawaki and Tsien, 2000; Erickson et al., 2001; Zheng et al., 2002, 2003). The efficiency of the energy transfer (E) depends on the distance, R, between the two fluorophores following the Forster equation:

$$E = (R_0)^6 / \left[(R_0)^6 + R^6 \right],$$

where R_0 is a spectroscopically determined distance when E = 0.5 (or 50% of FRET efficiency). Our FRET experiments involved passing fluorescence signal of the cell through a slit of a spectrograph and obtaining the spectrum of the fluorescence (Fig. 3 A). The spectra obtained by using the cerulean excitation wavelength (wavelength centered at 436 nm) and that obtained by using the eYFP excitation wavelength (wavelength centered at 500 nm) were from cells transfected with constructs containing cerulean and eYFP, or from cells transfected with constructs containing eYFP only. FRET efficiency was calculated using the method and equations demonstrated in Bykova et al. (2006). The FRET analysis is illustrated in Fig. 3 B. In brief, from cells transfected with cDNA constructs containing eYFP only, ratio A_0 is defined as the ratio between the fluorescence excited by light filtered by Cube I ($F^{Y(Direct)}_{436}$) and the fluorescence excited by the light passing filter Cube II (F^{Y}_{500}). Namely:

$$\text{Ratio } A_0 = F^{Y(Direct)}_{436} / F^{Y}_{500}.$$

Another ratio (Ratio A) was determined from cells cotransfected with constructs containing cerulean and eYFP. In this case, the cerulean fluorescence by direct excitation was obtained from cells expressing cerulean only, and was subtracted from the cerulean–excitation spectrum obtained from cells coexpressing cerulean and eYFP. The resulted spectrum only contains emission from the acceptor (eYFP), which includes two components: the eYFP emission caused by FRET ($F^{Y(FRET)}_{436}$) and the emission caused by direct excitation of eYFP ($F^{Y(Direct)}_{436}$). Thus,

$$\text{Ratio A} = F^{Y}_{436} / F^{Y}_{500} = \left(F^{Y(FRET)}_{436} + F^{Y(Direct)}_{436} \right) / F^{Y}_{500}.$$

We defined FRET ratio (FR) as the ratio of A and A_0:

$$\text{FR} = \text{Ratio A}/\text{Ratio A}_0 = \left(F^{Y(FRET)}_{436} + F^{Y(Direct)}_{436} \right) / F^{Y(Direct)}_{436} = 1 + F^{Y(FRET)}_{436} / F^{Y(Direct)}_{436}.$$

The apparent FRET efficiency (E_{app}) is calculated according to:

$$E_{app} = (\varepsilon_Y / \varepsilon_C) \times (FR - 1),$$

where ε_C and ε_Y are molar extinction coefficients of cerulean and eYFP, respectively.

Biochemical experiments and Western blots

The Flag-tagged CLC-0 constructs were transfected into HEK293 cells, and the cells were harvested 2 d after transfection. The harvested cells were lysed in Dulbecco's phosphate-buffered saline (Life Technologies) containing 25 mM 3-[(3-cholamidopropyl) dimethylammonio]-1-propanesulfonate (CHAPS) and a protease inhibitor cocktail (Roche). The supernatant of the lysate after centrifugation was treated with or without 10 µM copper phenanthroline before being loaded into a 7.5% SDS-PAGE gel for

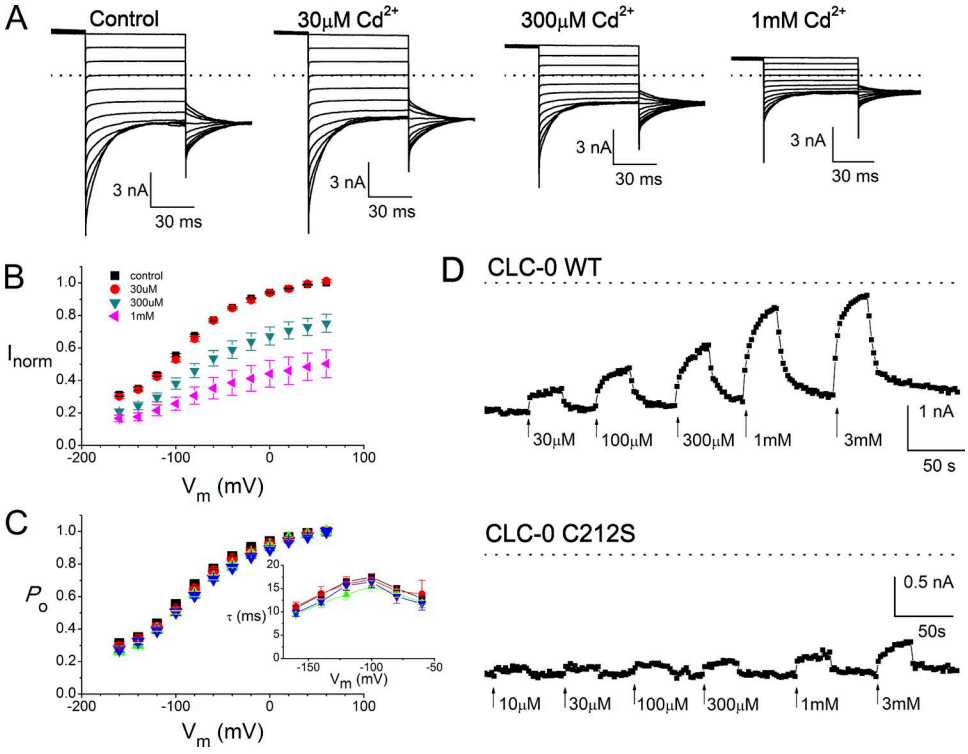

Figure 2. Intracellular Cd^{2+} inhibition on WT CLC-0 and the C212S mutant. (A) Original recording traces of WT CLC-0 in various intracellular [Cd^{2+}]. The current relaxations at those hyperpolarized voltages are caused by voltage-dependent closure of the fast gate. (B) Normalized steady-state current of WT CLC-0 in different intracellular [Cd^{2+}]: 0 (black), 30 µM (red), 300 µM (green), and 1 mM (purple). The initial tail currents after different test voltages in various [Cd^{2+}] were all normalized to the maximal initial tail current in 0 [Cd^{2+}]. (C) Fast-gate P_o as a function of voltage in the presence of 0 (black), 30 µM (red), 100 µM (green), and 300 µM (blue) Cd^{2+}, calculated by normalizing the initial tail current to the maximal tail current in the same [Cd^{2+}]. (Inset) Current relaxation time constant of the recorded current as those shown in A, which is equal to the inverse of the sum of the opening and the closing rate of the fast gate. The colors representing various [Cd^{2+}] are the same as those in the P_o-V plot. (D) Comparing the effects of intracellular Cd^{2+} between WT CLC-0 and the C212S mutant. A test pulse of 60 mV followed by a tail voltage at −100 mV was given every 2 s to monitor the Cd^{2+} inhibition. Current was measured at the end of the tailed pulse when the current reached the steady state. Various [Cd^{2+}] were applied at the time indicated by the arrows. Dash line represents zero-current level.

electrophoresis. The proteins were then transferred to nitrocellulose papers and detected by anti-Flag antibody (M2 antibody; Sigma-Aldrich).

RESULTS

Similar to the extracellular effect of Zn^{2+} on CLC-0 (Chen, 1998), intracellular Cd^{2+} can also inhibit the channel, although much higher concentrations, at least tens of micromolars, are required to generate inhibition (Fig. 2, A and B). The P_o-V curve and the kinetics of the fast gating of CLC-0 appear not to be affected by intracellular Cd^{2+} at a concentration range that significantly inhibits the channel (Fig. 2 C). Furthermore, the inhibition of the channel by Cd^{2+} is largely suppressed by the C212S mutation (Fig. 2 D), which prevents the slow gate of CLC-0 from closing (Lin et al., 1999). Collectively, these results suggest that intracellularly applied Cd^{2+} inhibits CLC-0 by modulating the slow gating.

The hypothesis that the intracellular Cd^{2+} inhibition of CLC-0 is mediated by modulating the channel's slow gating is consistent with the findings that the inhibition and recovery processes are slow (see Fig. 2 D, top). The slow kinetics of the inhibition rendered a precise characterization of the Cd^{2+} effect technically challenging because of relatively short durations of stable excised inside-out patch recordings of WT CLC-0. The problem was circumvented by an accidental finding that the mutations of I225W and V490W accelerated the inhibition kinetics. Mutations of the corresponding residues in CLC-ec1 (I201W/I422W) have been shown previously to disrupt the subunit interaction, resulting in functional monomeric CLC-ec1 proteins (Robertson et al., 2010). However, the I225W/V490W mutant of CLC-0 remains as a dimer when expressed in HEK293 cells, as shown by the FRET experiment in which the FRET efficiency between a FRET donor and a FRET acceptor attached to the I225W/V490W mutant is no less than that observed in the WT construct (Fig. 3, C and D). Nevertheless, the voltage dependence of the opening of the I225W/V490W mutant channel is opposite to that of the WT channel: the mutant channel's open probability (P_o) increases as the membrane voltage hyperpolarizes (Fig. 4 A). Moreover, Cd^{2+} inhibition is now faster and more potent: even 1 µM Cd^{2+} significantly inhibits the current (Fig. 4 B).

A full characterization of the Cd^{2+} sensitivity of I225W/V490W is shown in Fig. 5 A, in which the currents of the mutant channel in excised membrane patches were recorded in various Cd^{2+} concentrations ($[Cd^{2+}]$). We noticed that Cd^{2+} appears to have two distinct effects. First, the voltage-dependent steady-state activation

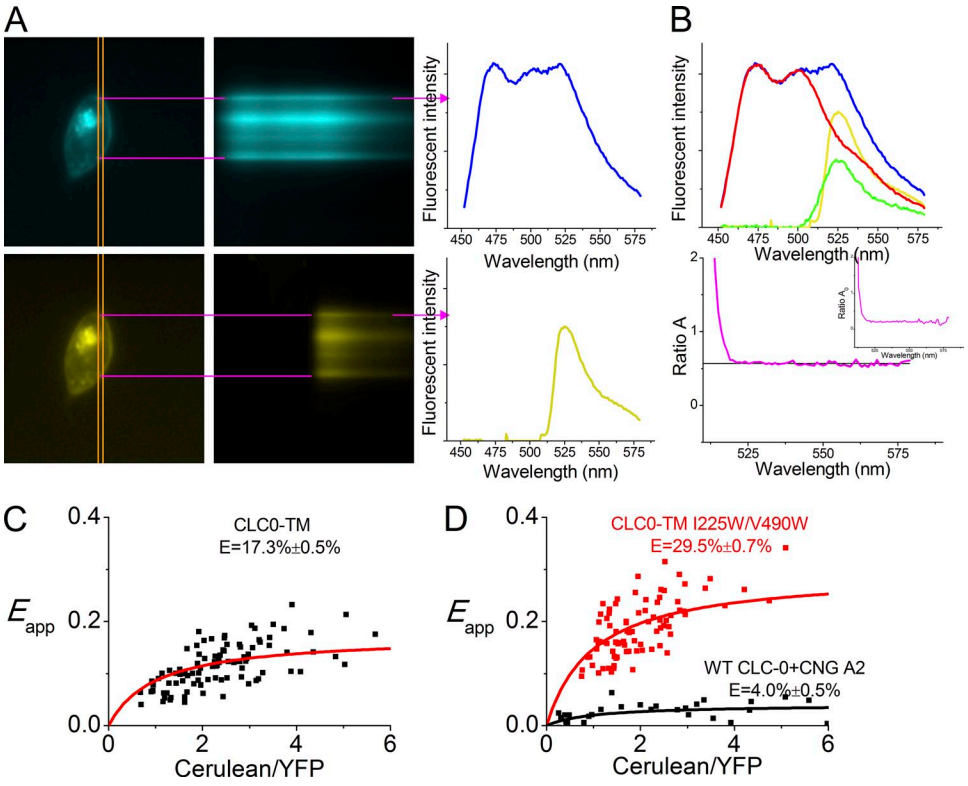

Figure 3. FRET experiments of the cerulean (C)- and eYFP (Y)-tagged CLC0-TM. (A) Fluorescence images of a cell expressing C- and Y-tagged CLC0-TM with I225W/V490W mutations from C (top left) and Y excitation (bottom left). The corresponding spectroscopic images (middle) were obtained by passing the signal through a slit (vertical orange lines). The emission spectra (right) were obtained from the upper edge of the spectroscopic images (arrows). (B; top) Emission spectra from the cell in A by C excitation (blue trace) and Y excitation (yellow trace). Red trace is the standard C emission spectrum from C excitation. Green trace was obtained by subtracting the red trace from the blue trace. (Bottom) Ratio A and Ratio A_0 (inset) are plotted against wavelength. (C) Apparent FRET efficiency (E_{app}) of the C- and Y-tagged CLC0-TM against the C/Y intensity ratio. Each point represents the E_{app} from a cell. (D) Apparent FRET efficiency of the C- and Y-tagged CLC0-TM with I225W/V490W mutations (red dots). Black dots were from a control experiment in which cells were cotransfected with WT CLC-0 and the subunit A2 of the rat olfactory CNG channel. Data points in C and D are fitted (solid curves) to Eqs. 3 and 4 of Bykova et al. (2006). In both C and D, significant FRET efficiency (~18% for WT and ~30% for I225W/V490W) was observed compared with the control experiment.

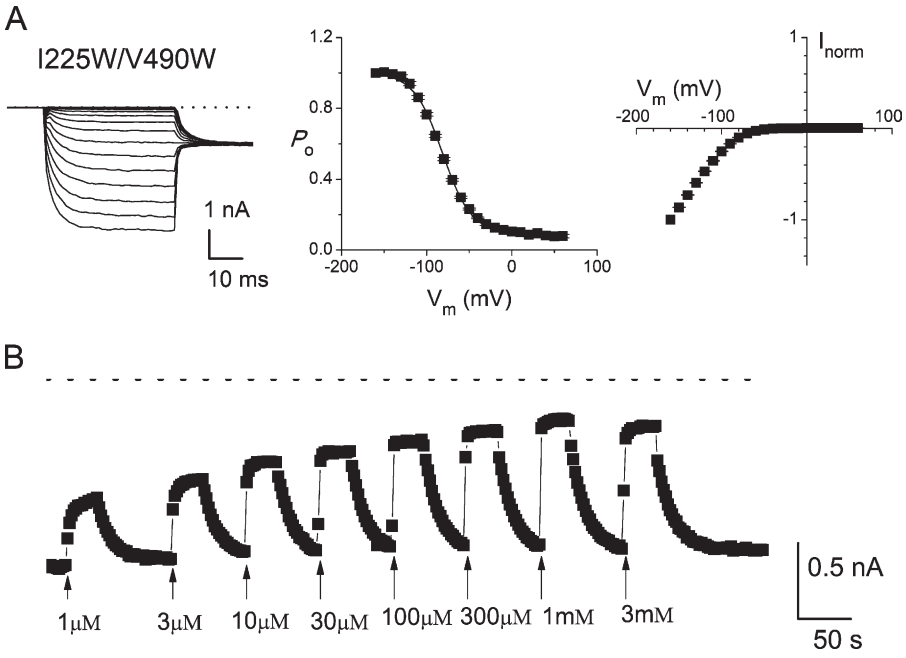

Figure 4. Intracellular Cd^{2+} inhibition of the I225W/V490W double mutant of CLC-0. (A) Original recording traces (left), steady-state voltage-dependent activation curve (middle), and the normalized steady-state I-V curve (right) of the I225W/V490W mutant. Data were from recording traces with p/4 leak subtraction. The dotted line in the left panel represents the zero-current level. (B) Effects of various intracellular [Cd^{2+}] on the steady-state current of the I225W/V490W mutant. A test pulse of −100 mV was given every 2 s, and the current was measured at the end of the pulse to monitor the Cd^{2+} inhibition. Dotted line represents the zero-current level. Cd^{2+} of various concentrations was applied as indicated by the arrows.

curve of this mutant shifts to more hyperpolarized voltages in low [Cd^{2+}] (<30 μM). Second, higher [Cd^{2+}] (such as 1 mM) reduces the maximal level of the channel activation (Fig. 5 B). Because of the dual effects of Cd^{2+}, the dose–response curve of the Cd^{2+} inhibition throughout the entire Cd^{2+} concentration range cannot be fitted to a single Langmuir function. We thus focused on the inhibition by low [Cd^{2+}] (up to 300 μM), and normalized the inhibition effect to that induced by 1 mM Cd^{2+}. The values of IC_{50} so obtained were 1, 7, and 204 μM at −80, −120, and −160 mV, respectively (Fig. 5 C). Therefore, the inhibition of I225W/V490W by Cd^{2+} is voltage dependent; the apparent affinity is decreased with more hyperpolarized membrane potentials.

To understand the structural basis of the Cd^{2+} inhibition, we searched for the amino acid residues involved in forming the Cd^{2+}-binding site. We first tested if cysteine-modifying reagents, such as MTS compounds, could affect Cd^{2+} inhibition because binding of transition metal ions in proteins frequently involves cysteine (Rulíšek and Vondrásek, 1998). Fig. 6 A shows that the Cd^{2+} inhibition of the I225W/V490W current, monitored by a 50-ms voltage pulse from 0 to −100 mV every 2 s, was indeed abolished after the patch was treated with intracellularly applied 2-(trimethylammonium)ethyl MTS (MTSET; Fig. 6 A, left) or 2-sulfonatoethyl MTS (MTSES) (Fig. 6 A, right). Consistently, the presence of intracellular Cd^{2+} reduced the effect of MTSET or

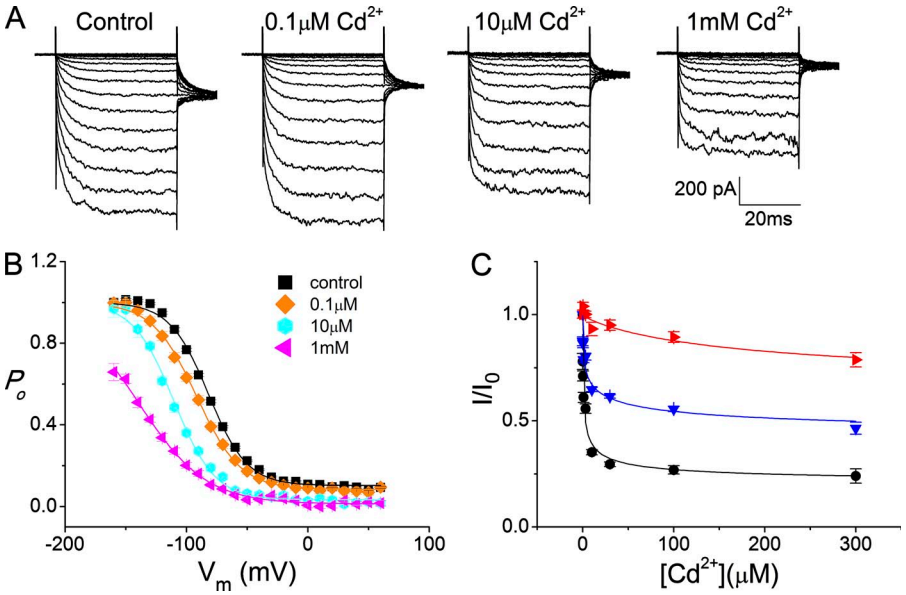

Figure 5. Steady-state inhibition of the I225W/V490W mutant of CLC-0 by intracellular Cd^{2+}. (A) Original recording traces in the absence of Cd^{2+} (control) and in the presence of various [Cd^{2+}]. (B) Voltage-dependent activation curves of I225W/V490W in 0 (control) and various [Cd^{2+}] based on the experiments similar to those shown in A. The initial tail current was normalized to that obtained after the test pulse of −160 mV in the absence of Cd^{2+}. Notice that the maximal P_o of I225W/V490W is reduced at 1 mM of Cd^{2+}. (C) Dose–response curves of the Cd^{2+} inhibition of I225W/V490W at different voltages (black, −80 mV; blue, −120 mV; red, −160 mV). Data points were fitted to a Langmuir equation with an apparent affinity of 1 μM (−80 mV), 7 μM (−120 mV), and 204 μM (−160 mV), respectively.

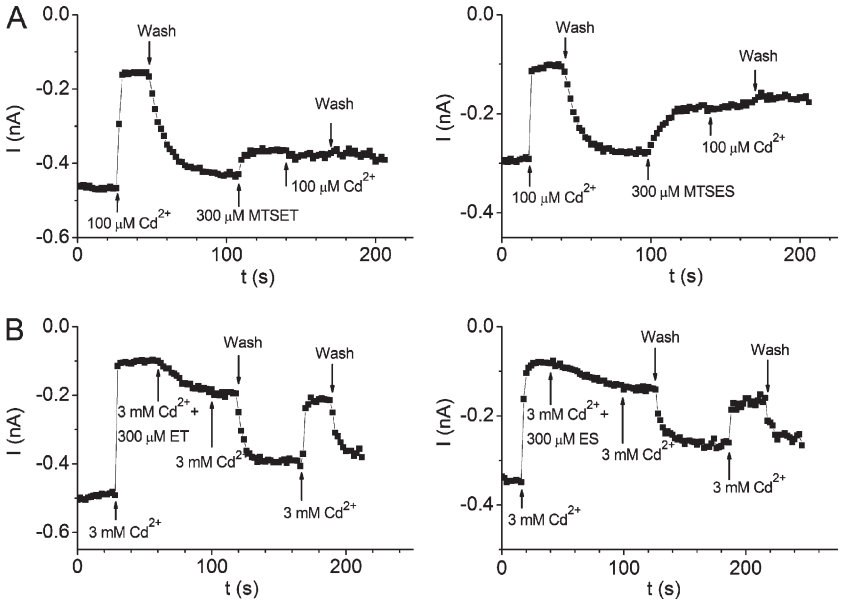

Figure 6. Competition between Cd^{2+} binding and the MTS modification in the I225W/V490W mutant of CLC-0. Current was monitored by a 40-ms test pulse of −100 mV every 2 s. MTS reagents and Cd^{2+} were applied or washed out at the time points indicated by arrows. (A) Modification of the I225W/V490W mutant with intracellular MTSET (left) or MTSES (right) suppresses the Cd^{2+} inhibition effect. (B) Cd^{2+} binding prevents the modification by MTSET (left) or MTSES (right) on the I225W/V490W mutant.

MTSES (Fig. 6 B), indicating that at least one cysteine forms part of the binding site, so that Cd^{2+} binding would protect the cysteine from MTS modifications.

Among the 12 endogenous cysteines in CLC-0, we have shown previously that C229, which is located at the dimer interface near the intracellular end of the transmembrane domain, can be modified by intracellular MTS reagents (Zhang et al., 2010). Interestingly, a histidine residue, H231, is located nearby, raising the possibility that it can act with C229 to coordinate Cd^{2+} as a bidentate ligand (Puljung and Zagotta, 2011). We thus tested whether C229 and H231 could both be involved in the formation of the Cd^{2+}-binding site. Mutating C229 (C229S), H231 (H231Y), or both (C229S/H231Y) in the background of I225W/V490W indeed suppressed the ability of Cd^{2+} to shift the steady-state activation curve (Fig. 7, A–C, respectively). When the C229S mutation was made in the WT CLC-0, the Cd^{2+} inhibition effect was also significantly reduced (Fig. 7 D). Likewise, the mutation H231Y also reduced the sensitivity of Cd^{2+} inhibition on WT CLC-0 (not depicted). However, the reduction of maximal channel activity by high [Cd^{2+}] still existed in these mutants (Fig. 7, A–D), suggesting that it is mediated by a different mechanism. Our results thus demonstrate that C229 and H231 form the high affinity Cd^{2+}-binding site, where binding of Cd^{2+}

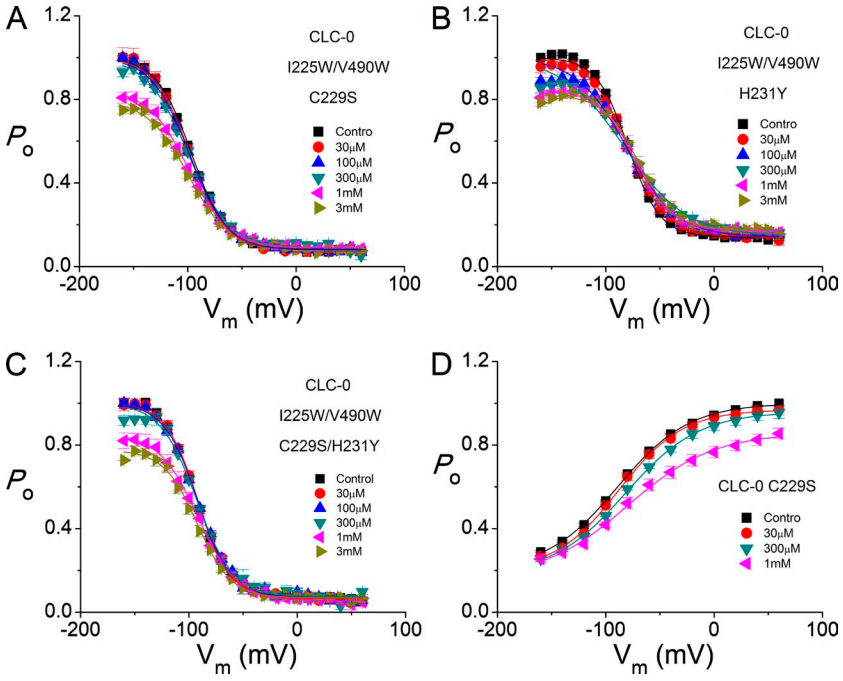

Figure 7. Mutations of C229 and/or H231 suppress the Cd^{2+} effect in shifting the P_o-V curve of I225W/V490W and WT CLC-0. (A–C) Steady-state P_o-V curves of I225W/V490W with the C229S single mutation (A), the H231Y single mutation (B), or the C229S/H231Y double mutations (C) in the presence of various [Cd^{2+}]. Notice that the shift of the P_o-V curve by Cd^{2+} is abolished, whereas the inhibition of the maximal P_o at high concentrations of Cd^{2+} is still present. (D) Steady-state P_o-V curves of the C229S mutant on the WT background in different [Cd^{2+}].

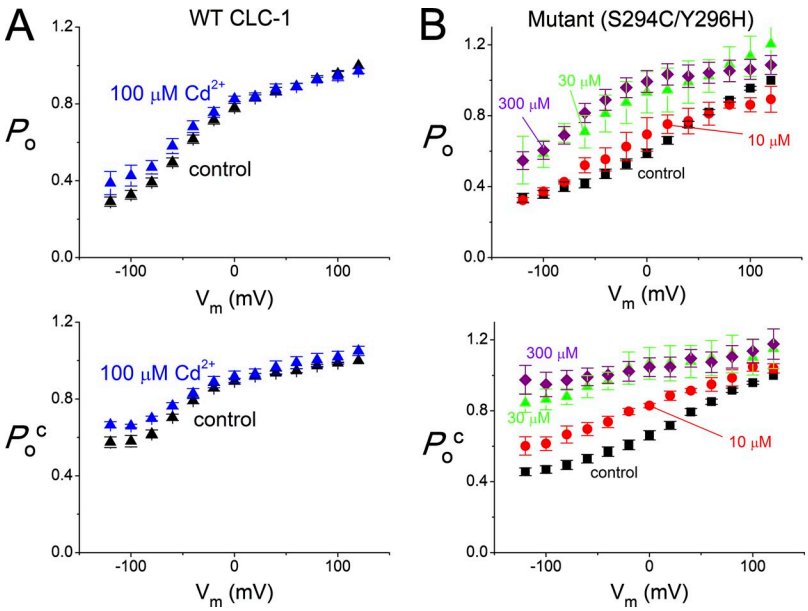

Figure 8. Introducing a cysteine and a histidine residue to positions in CLC-1 that correspond to C229 and H231 of CLC-0 enables a modulation of CLC-1 by micromolar [Cd^{2+}]. (A) The overall channel open probability (P_o; top) and the common-gate open probability (P_o^c; bottom) of WT CLC-1 as a function of voltage in the absence (control, black) and presence of 100 μM Cd^{2+} (blue). (B) The P_o–V and P_o^c–V curves of the S294C/Y296H mutant of CLC-1 in various intracellular [Cd^{2+}]. C229 and H231 of CLC-0 are not conserved in CLC-1, and as expected, 100 μM Cd^{2+} has nearly no effect on WT CLC-1 (Fahlke et al., 1998). However, 10 μM Cd^{2+} significantly increases the open probability of the common gate (P_o^c) of the CLC-1 mutant S294C/Y296H. Notice the opposite effect of Cd^{2+} on the open probability of CLC-1 (potentiation) compared with that of CLC-0 (inhibition).

shifts the steady-state activation curve of I225W/V490W. It is likely that C229 and H231 from both CLC-0 subunits together coordinate Cd^{2+} binding, as these residues are located near the dimer interface and therefore are close to each other (see Fig. 1). The conclusion that C229 and H231 form the Cd^{2+}-binding site is further supported by experiments from CLC-1. These two residues are not conserved in CLC-1, which is not sensitive to intracellular Cd^{2+} modulation (Figs. 8 A and 9 A). When cysteine and histidine were introduced to the corresponding positions in CLC-1 (S294C/Y296H), a Cd^{2+}-binding site was created, and the activation of CLC-1 could be modulated by intracellular Cd^{2+} (Figs. 8 B and 9, A and B). Like the MTS modification of the endogenous cysteine (C229) in CLC-0, modification of the introduced cysteine (S294C) abolished Cd^{2+} inhibition on CLC-1 containing the engineered Cd^{2+}-binding site (Fig. 9 C).

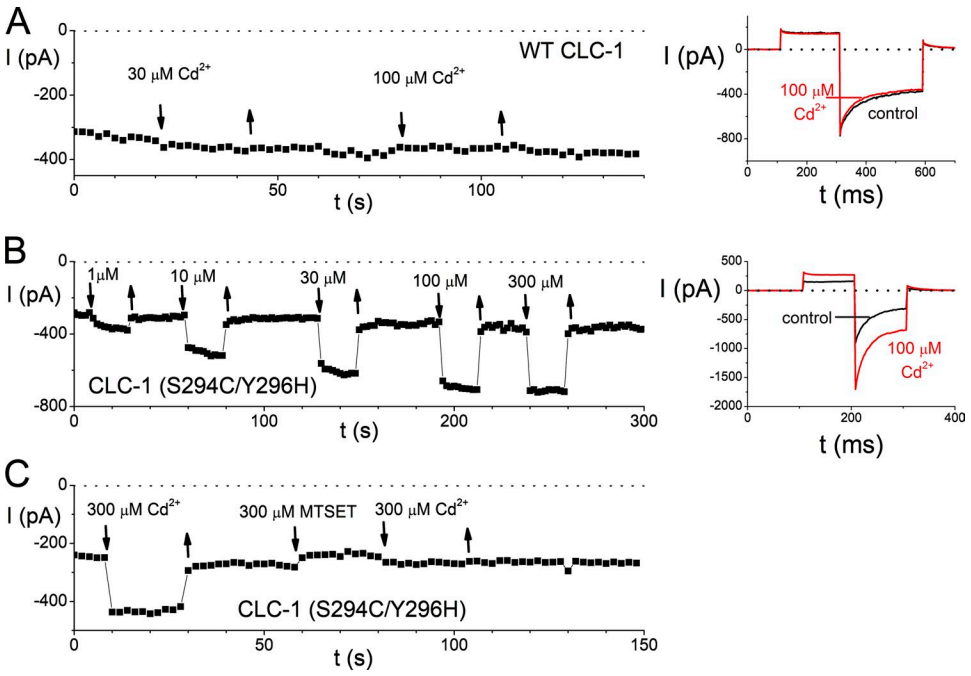

Figure 9. Suppressing the Cd^{2+} effect in the S294C/Y296H mutant of CLC-1 by intracellular MTS reagents. (A) Micromolar concentrations of intracellular Cd^{2+} have little effect on the WT CLC-1. The current was monitored continuously by a pulse of 60 mV followed by a voltage step at −100 mV. Intracellular Cd^{2+} was applied (downward arrows) and washed out (upward arrows) as indicated. Inset shown on the right panel is a comparison of two original recording traces taken before (black) and after (red) the application of 100 μM Cd^{2+}. (B) Intracellular Cd^{2+} potentiates the current of the S294C/Y296H double mutant of CLC-1. Inset on the right is a comparison of two original recording traces taken before (black) and after (red) 100 μM [Cd^{2+}]. Notice that the current deactivation kinetics at the hyperpolarization voltage caused by the closure of the fast gate is not altered by Cd^{2+}, indicating that the effect is not on the fast gating of the channel. (C) Potentiation of the S294C/Y296H mutant by intracellular Cd^{2+} is abolished after modifying the channel with intracellular MTSET, indicating that the introduced cysteine and histidine at the positions of S294 and Y296 form a Cd^{2+}-binding site in CLC-1 as well.

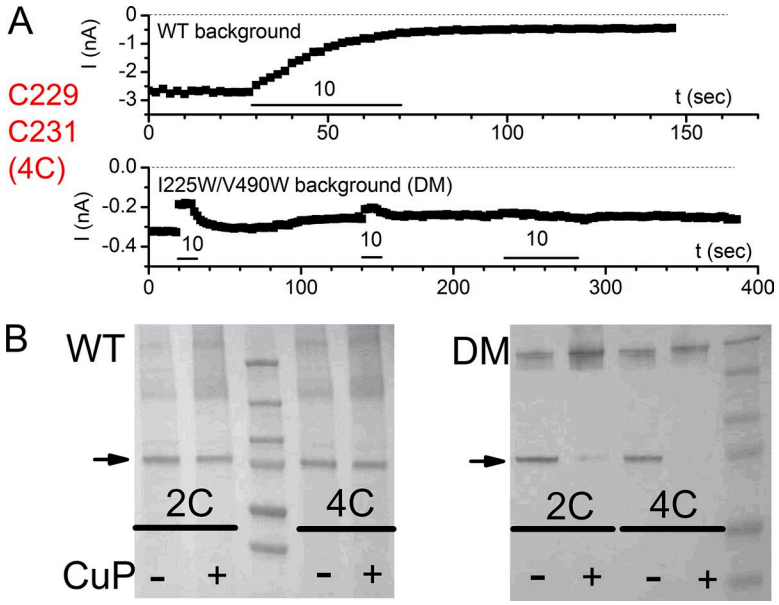

Figure 10. Disulfide bond linking two CLC subunits. (A) Inhibition of CLC-0 by Cd^{2+} binding to the binding site containing four cysteines in the WT CLC-0 background (top) and the dimer interface mutant background (DM; bottom). Excised inside-out patch recordings. The voltage pulse (60 mV followed by −100 mV) for monitoring the current was given every 2 s, and the current at the end of the −100-mV voltage was monitored. Dotted lines, zero current level. Horizontal bars indicate the application of 10 µM Cd^{2+}. (B) I229W/V490W dimer interface mutations (DM) facilitate disulfide bond formation in copper phenanthroline (CuP) between the two C231 residues. "4C" indicates that all four positions at positions 229 and 231 from two subunits were cysteine, whereas "2C" contained cysteine only at position 231 but not at position 229 (C229S/H231C). Arrows indicate the monomer of CLC-0, which disappeared likely because of a disulfide bond formation between the two C231 residues.

Because binding sites for transition metal cations can be formed by four cysteine residues (Yellen et al., 1994), we tested the effect of Cd^{2+} on CLC-0 with the H231C mutation. Such a CLC-0 construct contains cysteine at all four positions of 229 and 231 from two subunits (and thus will be called "4C" mutant). In the WT background, the 4C mutant becomes very sensitive to Cd^{2+}, and the Cd^{2+} inhibition is nearly irreversible (Fig. 10 A, top). Cd^{2+} inhibition of the 4C mutant with I225W/V490W background mutations, however, is very different; the inhibition can be quickly washed out, but with the time of patch excision the channel is less and less sensitive to Cd^{2+} (Fig. 10 A, bottom). We suspected that this time-dependent reduction of Cd^{2+} sensitivity might result from the formation of a disulfide bond among these four cysteine residues after patch excision, which could change the oxidation/reduction condition of the channel (Zhang et al., 2008). Indeed, Western blots shown in Fig. 10 B demonstrate that the monomeric band of the 4C mutant in the I225W/V490W background disappeared after oxidation (Fig. 10 B, right). On the other hand, the majority of the 4C mutant in the WT CLC-0 background still remained as monomers in the SDS gel after copper phenanthroline treatment (Fig. 10 B, left). Similar results were observed in a "2C" mutant in which cysteine was present only at position 231 but not at position 229 (Fig. 10 B), suggesting that it is the two cysteines at position 231 that form a disulfide bond. Thus, through the differences in Cd^{2+} inhibition and disulfide bond formation, we demonstrate that like the WT Cd^{2+}-binding site, the structure of the mutant Cd^{2+}-binding site with four cysteines is changed by the I225W/V490W mutations.

Because C229 and H231 are located near the intracellular end of the transmembrane domain and interactions between the transmembrane domain and the cytoplasmic domain have been demonstrated in CLC molecules (Feng et al., 2010; Bennetts and Parker, 2013), the cytoplasmic domain of CLC-0 may influence Cd^{2+} inhibition. We thus tested the intracellular Cd^{2+} effect on a CLC-0

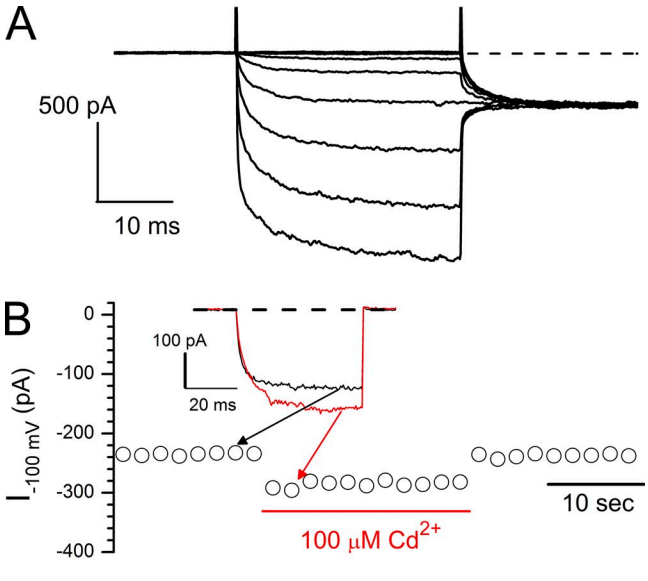

Figure 11. Effects of intracellular Cd^{2+} on the C terminus–truncated CLC-0 (CLC0-TM). (A) Current of the eYFP-tagged CLC0-TM activated by a voltage family from 60 to −160 mV in a −20-mV voltage step. Excised inside-out patch recordings. Tail voltage was −100 mV. (B) Effects of intracellular Cd^{2+} on the current of CLC0-TM monitored by continuously applying a voltage pulse of −100 mV (40 ms) every 2 s. Currents at the end of the −100-mV voltage step are plotted against time. 100 µM Cd^{2+} was applied as indicated by the horizontal red line. (Inset) Comparison of the recording traces before and after Cd^{2+} application. Dashed line indicates the zero-current level.

mutant in which the C-terminal region of the channel after residue 530 is replaced with a fluorescent protein. As reported previously (Bykova et al., 2006), this CLC-0 mutant (abbreviated as "CLC0-TM") generates hyperpolarization-activated currents (Fig. 11 A). Interestingly, Cd^{2+} did not inhibit but potentiated this mutant (Fig. 11 B), suggesting that the cytoplasmic domain of the CLC channel may also be involved in the intracellular Cd^{2+} modulation, likely through its interaction with the transmembrane domain.

To gain further insights into the Cd^{2+} modulation mechanism, we studied the kinetics of Cd^{2+} inhibition on I225W/V490W of CLC-0, taking advantage of the faster kinetics of Cd^{2+} inhibition in this mutant. Fig. 12 A illustrates a two-pulse protocol used to examine the rate of Cd^{2+} inhibition by measuring the current of the I225W/V490W mutant elicited by a −100-mV voltage pulse before (first pulse) and after the patch was exposed to Cd^{2+} for a certain amount of time (second pulse). Combining multiple recording traces from the same patch generates the time course of Cd^{2+} inhibition (Fig. 12 B). It is worth noticing that there appears to be a delay of the current inhibition because the current recorded after applying Cd^{2+} for 0.2 s is almost the same as that before the Cd^{2+} application. This delay has little voltage dependence (Fig. 12 C), but as $[Cd^{2+}]$ is increased, the delay is shortened (Fig. 12 D). To analyze the kinetics of Cd^{2+} inhibition like that shown in Fig. 12 B, we normalized the current induced by the second voltage pulse to the current before Cd^{2+} application, and plotted the time course of the current inhibition by Cd^{2+} (Fig. 13 A). Fitting the Cd^{2+} inhibition time course with an exponential function gives the inhibition time constant (τ_{on}), the inverse of which ($1/\tau_{on}$) is defined as the apparent Cd^{2+} inhibition rate (or apparent on rate), k_{on}. The observation that k_{on} is a saturable function of $[Cd^{2+}]$ (Fig. 13 B) suggests that Cd^{2+} inhibition is not a simple bimolecular reaction involving only Cd^{2+} binding. These results suggest that the binding of Cd^{2+} to the open-state channel may not immediately close the channel, and the delay in current inhibition upon Cd^{2+} application could result from the conformational change between the open and the closed state of this dimer interface mutant.

We have also measured the rate of current recovery after Cd^{2+} washout (apparent off-rate, or k_{off}) using a similar two-pulse protocol. The current recovery process was well described by a single-exponential function (recording traces not depicted). These kinetic measurements of Cd^{2+} inhibition and recovery were conducted at multiple holding voltages (Fig. 13, C and D). The values of the apparent τ_{on} (in 30 µM Cd^{2+}) and τ_{off} at 0, −40, and −80 mV are compared in Fig. 13 E. Although τ_{on} is insensitive to the change of membrane potential, the value of τ_{off} decreases as membrane potential becomes more negative. Therefore, the lower apparent affinity of Cd^{2+} inhibition at more negative voltages on the I225W/V490W mutant results mostly from a faster off-rate by membrane hyperpolarization. Collectively, these results suggest a state-dependent

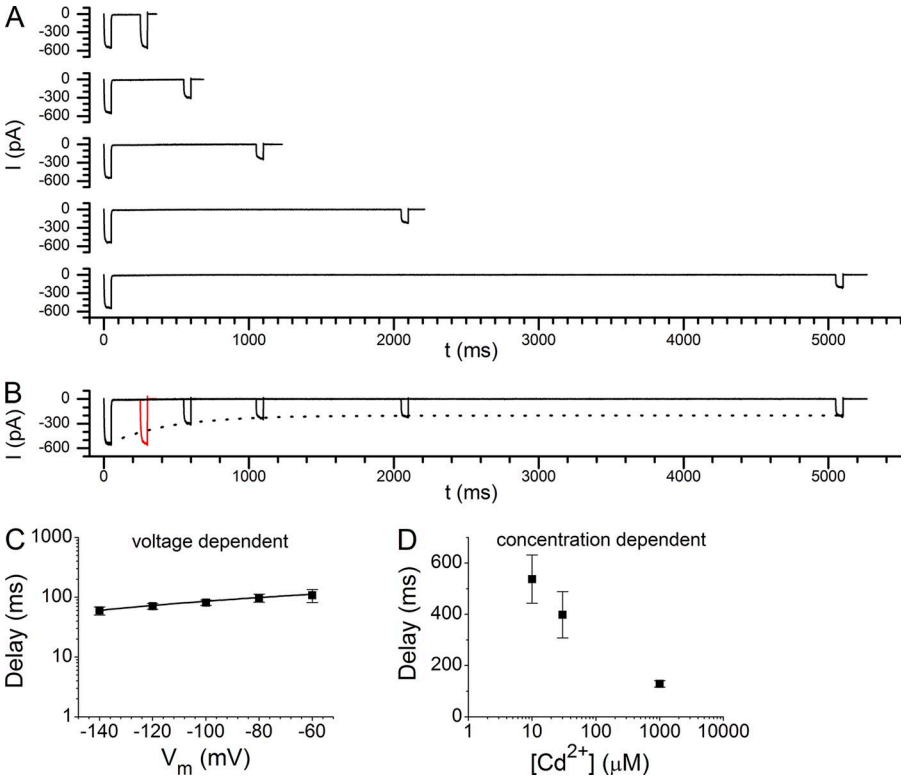

Figure 12. Rate of Cd^{2+} inhibition (on rate) on the I225W/V490W mutant of CLC-0. (A) Original recording traces from one patch using the two-pulse (to −100 mV) protocol described in Materials and methods. $[Cd^{2+}]$ = 100 µM. V_{hold} = −40 mV. (B) Combining the recording traces from A shows the time course of Cd^{2+} inhibition. Dotted curve is the single-exponential fit of the current amplitude elicited at various time spots except the one at 0.2 s (the second pulse). Notice the delay of Cd^{2+} inhibition shown by comparing the second pulse (in red) with the entire inhibition time course. (C) Delay of current inhibition upon Cd^{2+} application obtained at different voltages. $[Cd^{2+}]$ = 300 µM. Solid curve is a voltage-dependent exponential fit for the relation between the delay time and the voltage, with an estimated electric distance of −0.025. n = 7. (D) $[Cd^{2+}]$ dependence of the delay of current inhibition. V_m = −80 mV. Data points are the average of five to eight experiments (mean ± SEM).

binding of Cd^{2+} to the channel; Cd^{2+} binding to the closed state of the channel is energetically more favored than the binding to the open state.

DISCUSSION

Transition metal ions have been widely used to study the structure–function relationship of ion channels. In the *Shaker* K^+ channel, for example, the state-dependent affinity change of extracellular Cd^{2+} inhibition revealed a structural change on the external mouth of the channel during the slow (C-type) inactivation (Yellen et al., 1994). Intracellularly applied Cd^{2+} was also used to show that the activation gate of the *Shaker* K^+ channel can be trapped in the open state when an intersubunit metal bridge is formed (Holmgren et al., 1998). CLC-0 and CLC-1 have been found to be inhibited by Zn^{2+} or Cd^{2+} applied from the extracellular side (Rychkov et al., 1997; Chen, 1998), and extracellular Zn^{2+} is known to inhibit WT CLC-0 by facilitating the closure of the slow gate (Chen, 1998). We found in the present study that the inhibition of WT CLC-0 by intracellular Cd^{2+} is likely mediated by a modulation of the slow gating of CLC-0 as well because intracellular Cd^{2+} has little effect on the fast gating of the channel (Fig. 2 C), and because the inhibition is largely suppressed by the C212S mutation (Fig. 2 D), which prevents the slow gate of CLC-0 from closing (Lin et al., 1999).

The apparent affinity of intracellular Cd^{2+} on WT CLC-0 is quite low—tens to hundreds of micromolars of $[Cd^{2+}]$ is required for an observable effect. However, the potency of Cd^{2+} is significantly enhanced by tryptophan substitutions of I225 and V490, which correspond to dimer interface residues I201 and I422, respectively, in CLC-ec1. The I201W/I422W mutation in CLC-ec1 disrupts dimer architecture, leading to the formation of CLC monomers (Robertson et al., 2010). The corresponding mutations in CLC-0, however, do not separate the two channel subunits as indicated by a high FRET efficiency between the FRET donor and acceptor tagged to the C termini of the transmembrane domains (Fig. 3). The formation of a disulfide bond between the two cysteine residues at position 231 further demonstrates a dimeric CLC molecule in the I290W/V490W background mutations (Fig. 10). Despite the fact that CLC-0 with I225W/V490W mutations remains as a dimer, the mutant channel's voltage-dependent gating properties have been inverted from that of the WT channel (Fig. 4 A). It is conceivable that introducing bulky tryptophan side chains into the dimer interface alters the interaction between the two CLC subunits, thus increasing apparent affinity and kinetics of Cd^{2+} inhibition (Fig. 4 B), and facilitating disulfide bond formation between cysteines at position 231 (Fig. 10).

A closer examination of the Cd^{2+} inhibition on the I225W/V490W mutant reveals that intracellular Cd^{2+}

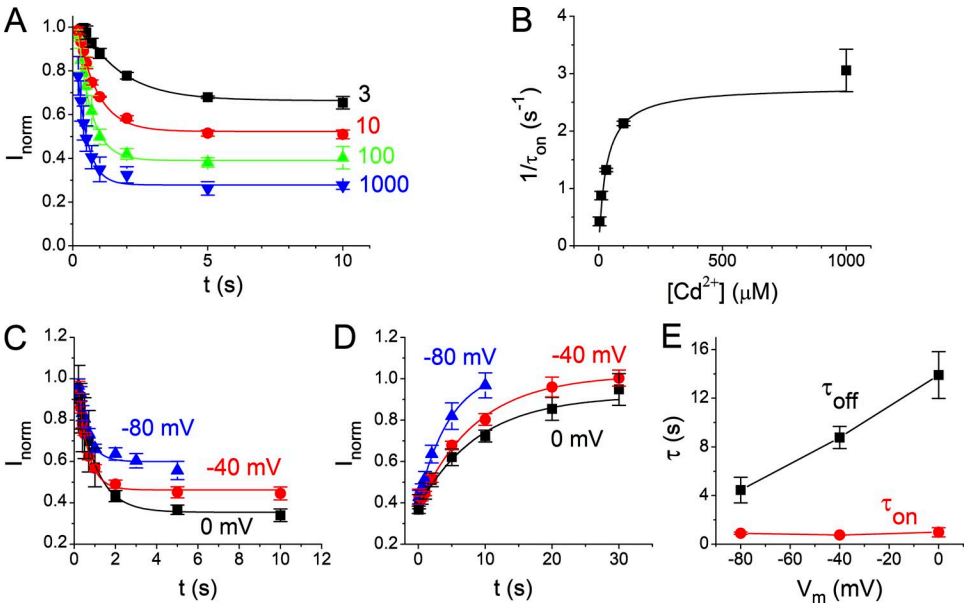

Figure 13. Voltage dependence of the inhibition and recovery kinetics of the Cd^{2+} modulation of the I225W/V490W mutant of CLC-0. (A) Time course of current inhibition by various $[Cd^{2+}]$ (in micromolars) at −40 mV. (B) Inverse of the time constant of Cd^{2+} inhibition ($k_{on} = 1/\tau_{on}$) as a function of $[Cd^{2+}]$. The values of τ_{on} were obtained from single-exponential fits as in A. (C) Averaged time course for the inhibition by 30 µM Cd^{2+} at 0, −40, and −80 mV. Data points were calculated by normalizing the current in various $[Cd^{2+}]$ to the control current ($[Cd^{2+}] = 0$). (D) Time course of the current recovery from Cd^{2+} inhibition. Data points were obtained by normalizing the current recovered after Cd^{2+} was washed out to that before the application of Cd^{2+}. (E) Time constants of the inhibition (τ_{on}) and recovery (τ_{off}) as a function of membrane voltage. Time constants were obtained by fitting the data points in C and D with single-exponential functions.

appears to have two effects. At low micromolar [Cd^{2+}], the mutant channel's steady-state activation curve is shifted to more hyperpolarized voltages by Cd^{2+}. We observed a competition between intracellular Cd^{2+} inhibition and MTS modification (Fig. 6), a clear indication that like many other transition metal-binding proteins, the amino acid cysteine is directly involved in forming the Cd^{2+}-binding site. Further mutagenesis experiments showed that the mutation of C229S, H231Y, or both abolishes the Cd^{2+}-induced shift of the steady-state activation curve in WT CLC-0 and in the I225W/V490W mutant (Fig. 7), indicating that the high affinity Cd^{2+} inhibition is mediated through the binding site formed by C229 and H231. On the other hand, the maximal open probability of these mutants was still inhibited by Cd^{2+} at the millimolar concentrations, suggesting that the low affinity Cd^{2+} inhibition may be mediated by a different mechanism.

The residues C229 and H231 of CLC-0 correspond to R205 and Q207, respectively, in CLC-ec1, which are in close proximity to the same residues in the partner subunit (Fig. 1). As seen in many metalloproteins, tetrahedral is a preferred coordination arrangement for Cd^{2+} binding, usually involving four cysteine/histidine residues (Rulíšek and Vondrásek, 1998). Therefore, it is likely that the Cd^{2+} site in CLC-0 is formed by two subunits, each contributing two chelators from C229 and H231 to bind Cd^{2+}. These cysteine and histidine residues, however, are not conserved in CLC-1, thus explaining the fact that WT CLC-1 is insensitive to intracellular Cd^{2+}, as shown in Figs. 8 A and 9 A, and also reported previously by others (Rychkov et al., 1997; Fahlke et al., 1998). In this study, we are able to construct a Cd^{2+}-binding site in CLC-1 by engineering S294C/Y296H mutations to mimic the Cd^{2+} site in CLC-0. This strategy yields a CLC-1 mutant whose activity is modulated by low micromolar intracellular Cd^{2+}, although the consequence of the Cd^{2+} modulation is potentiation but not inhibition of the channel current! Such Cd^{2+} effect, again, is abolished by pretreating the channel with intracellular MTS reagents (Fig. 9 C), indicating that a Cd^{2+}-binding site is indeed created. Previous studies have indicated an interaction of the transmembrane domain and the C-terminal cytoplasmic domain of CLC proteins (Feng et al., 2010; Bennetts and Parker, 2013). Experiments in Fig. 11 show that removing the C-terminal region of CLC-0 changes the Cd^{2+} effect from inhibition to potentiation. Thus, the interaction of the transmembrane domain with the C-terminal cytoplasmic domain as well as the subunit interaction at the dimer interface are both involved in intracellular Cd^{2+} modulation of CLC-0.

These experimental results thus allow us to compare the functional roles of subunit interactions between CLC channels and bacterial CLC proteins. It was demonstrated previously that cross-linking the two CLC-ec1 subunits covalently poses little impact on the Cl^- transport function (Nguitragool and Miller, 2007). Similarly, the fast gating of CLC-0 and CLC-1 is not affected by restricting molecular motions at the dimer interface with Cd^{2+} (Figs. 2 and 9). This is consistent with the accepted concept that the Cl^-/H^+ exchange cycle of CLC-ec1 and the fast gating of CLC channels are homologous, mediated by molecular motions (for example, swinging of the glutamate side chain) confined in individual subunits. Coordinating opening and closing of the two Cl^- pathways requires the slow/common gating mechanism that enables the cross talk of the two subunits through the dimer interface. Cd^{2+} binding or the introduction of bulky residues at the dimer interface would perturb such a cross talk and thus modulate slow/common gating of CLC channels. It is possible that mutation of I225W and V490W speeds up the inactivation of CLC-0 (closure of the slow gate), explaining the faster kinetics of Cd^{2+} inhibition in the I225W/V490W double mutant than in the WT channel. Interestingly, Cd^{2+} binding inhibits the current of WT CLC-0 and I225W/V490W but potentiates the current of CLC0-TM (Fig. 11) and the CLC-1 mutant S294C/Y296H (Figs. 8 and 9). The different consequences of Cd^{2+} binding (potentiation vs. inhibition of the current) may result from the difference between the cross talk of the two subunits in these various channels. Another possibility is that the allosteric interactions between the Cd^{2+}-binding site and the C-terminal cytoplasmic domain are different in these channels. It will await further studies to understand the different functional consequences of Cd^{2+} modulations in CLC-0, CLC-1, and the C terminus–truncated CLC channel.

If C229 and H231 of CLC-0 are located at the intracellular end of the transmembrane domain, like their corresponding residues R205 and Q207 in CLC-ec1 (Fig. 1), it is expected that the Cd^{2+} site would be outside the transmembrane electric field, and thus Cd^{2+} binding should be voltage independent. Indeed, the apparent on-rate of Cd^{2+} is voltage independent (Fig. 13 E). However, the apparent Cd^{2+} affinity is lower at more hyperpolarized voltages (Fig. 5 C) because membrane hyperpolarization (which favors the opening of the I225W/V490W mutant) accelerates Cd^{2+} dissociation (Fig. 13, D and E). The voltage dependence of the apparent off-rate thus suggests a state-dependent Cd^{2+} inhibition; namely, Cd^{2+} binding to the open state is energetically less favorable than the binding to the closed state. Furthermore, Cd^{2+} inhibition shows an appreciable delay (Fig. 12) and the apparent on-rate of Cd^{2+} inhibition is a saturable function of [Cd^{2+}] (Fig. 13 B), both corroborating the idea that Cd^{2+} binding to the open-state channel cannot immediately shut the pore. Instead, it will require a subsequent molecular event, likely a conformational change associated with slow gating, to close the channel.

In summary, we have characterized the inhibition of CLC-0's slow gating by intracellular Cd^{2+}, and have identified a Cd^{2+}-binding site formed by C229 and H231 at the intracellular end of the dimer interface of the transmembrane domain. We have also shown that the residues I225 and V490 of CLC-0, like the corresponding residues in other CLC channels, are important for the channel gating mechanism likely because of their roles in the subunit interaction. Binding of Cd^{2+} to the dimer interface and mutations of dimer interface residues thus may modulate the slow/common gating of CLC channels by altering subunit interactions.

We would like to thank Drs. Robert Fairclough and Tzyh-Chang Hwang for critical readings of the manuscript.

This work was supported by a grant from National Institutes of Health (R01GM065447) and by the Jong L. Chen Family Neuroscience Research Fund.

The authors declare no competing financial interests.

Merritt C. Maduke served as editor.

Submitted: 17 April 2015
Accepted: 9 November 2015

REFERENCES

Accardi, A., and M. Pusch. 2000. Fast and slow gating relaxations in the muscle chloride channel CLC-1. *J. Gen. Physiol.* 116:433–444. http://dx.doi.org/10.1085/jgp.116.3.433

Bennetts, B., and M.W. Parker. 2013. Molecular determinants of common gating of a ClC chloride channel. *Nat. Commun.* 4:2507. http://dx.doi.org/10.1038/ncomms3507

Bennetts, B., G.Y. Rychkov, H.L. Ng, C.J. Morton, D. Stapleton, M.W. Parker, and B.A. Cromer. 2005. Cytoplasmic ATP-sensing domains regulate gating of skeletal muscle ClC-1 chloride channels. *J. Biol. Chem.* 280:32452–32458. http://dx.doi.org/10.1074/jbc.M502890200

Bykova, E.A., X.D. Zhang, T.Y. Chen, and J. Zheng. 2006. Large movement in the C terminus of CLC-0 chloride channel during slow gating. *Nat. Struct. Mol. Biol.* 13:1115–1119. http://dx.doi.org/10.1038/nsmb1176

Chen, T.Y. 1998. Extracellular zinc ion inhibits ClC-0 chloride channels by facilitating slow gating. *J. Gen. Physiol.* 112:715–726. http://dx.doi.org/10.1085/jgp.112.6.715

Chen, T.Y. 2005. Structure and function of clc channels. *Annu. Rev. Physiol.* 67:809–839. http://dx.doi.org/10.1146/annurev.physiol.67.032003.153012

Duffield, M., G. Rychkov, A. Bretag, and M. Roberts. 2003. Involvement of helices at the dimer interface in ClC-1 common gating. *J. Gen. Physiol.* 121:149–161. http://dx.doi.org/10.1085/jgp.20028741

Dutzler, R., E.B. Campbell, M. Cadene, B.T. Chait, and R. MacKinnon. 2002. X-ray structure of a ClC chloride channel at 3.0 Å reveals the molecular basis of anion selectivity. *Nature.* 415:287–294. http://dx.doi.org/10.1038/415287a

Dutzler, R., E.B. Campbell, and R. MacKinnon. 2003. Gating the selectivity filter in ClC chloride channels. *Science.* 300:108–112. http://dx.doi.org/10.1126/science.1082708

Erickson, M.G., B.A. Alseikhan, B.Z. Peterson, and D.T. Yue. 2001. Preassociation of calmodulin with voltage-gated Ca^{2+} channels revealed by FRET in single living cells. *Neuron.* 31:973–985.

Estévez, R., and T.J. Jentsch. 2002. CLC chloride channels: correlating structure with function. *Curr. Opin. Struct. Biol.* 12:531–539. http://dx.doi.org/10.1016/S0959-440X(02)00358-5

Fahlke, C., T.H. Rhodes, R.R. Desai, and A.L. George Jr. 1998. Pore stoichiometry of a voltage-gated chloride channel. *Nature.* 394:687–690. http://dx.doi.org/10.1038/29319

Feng, L., E.B. Campbell, Y. Hsiung, and R. MacKinnon. 2010. Structure of a eukaryotic CLC transporter defines an intermediate state in the transport cycle. *Science.* 330:635–641. http://dx.doi.org/10.1126/science.1195230

Holmgren, M., K.S. Shin, and G. Yellen. 1998. The activation gate of a voltage-gated K^+ channel can be trapped in the open state by an intersubunit metal bridge. *Neuron.* 21:617–621. http://dx.doi.org/10.1016/S0896-6273(00)80571-1

Jentsch, T.J. 2008. CLC chloride channels and transporters: From genes to protein structure, pathology and physiology. *Crit. Rev. Biochem. Mol. Biol.* 43:3–36. http://dx.doi.org/10.1080/10409230701829110

Jentsch, T.J., I. Neagoe, and O. Scheel. 2005. CLC chloride channels and transporters. *Curr. Opin. Neurobiol.* 15:319–325. http://dx.doi.org/10.1016/j.conb.2005.05.002

Kubisch, C., T. Schmidt-Rose, B. Fontaine, A.H. Bretag, and T.J. Jentsch. 1998. ClC-1 chloride channel mutations in myotonia congenita: Variable penetrance of mutations shifting the voltage dependence. *Hum. Mol. Genet.* 7:1753–1760. http://dx.doi.org/10.1093/hmg/7.11.1753

Lin, C.W., and T.Y. Chen. 2003. Probing the pore of ClC-0 by substituted cysteine accessibility method using methane thiosulfonate reagents. *J. Gen. Physiol.* 122:147–159. http://dx.doi.org/10.1085/jgp.200308845

Lin, Y.W., C.W. Lin, and T.Y. Chen. 1999. Elimination of the slow gating of ClC-0 chloride channel by a point mutation. *J. Gen. Physiol.* 114:1–12. http://dx.doi.org/10.1085/jgp.114.1.1

Ludewig, U., M. Pusch, and T.J. Jentsch. 1996. Two physically distinct pores in the dimeric ClC-0 chloride channel. *Nature.* 383:340–343. http://dx.doi.org/10.1038/383340a0

Maduke, M., C. Miller, and J.A. Mindell. 2000. A decade of CLC chloride channels: Structure, mechanism, and many unsettled questions. *Annu. Rev. Biophys. Biomol. Struct.* 29:411–438. http://dx.doi.org/10.1146/annurev.biophys.29.1.411

Middleton, R.E., D.J. Pheasant, and C. Miller. 1994. Purification, reconstitution, and subunit composition of a voltage-gated chloride channel from *Torpedo* electroplax. *Biochemistry.* 33:13189–13198. http://dx.doi.org/10.1021/bi00249a005

Middleton, R.E., D.J. Pheasant, and C. Miller. 1996. Homodimeric architecture of a ClC-type chloride ion channel. *Nature.* 383:337–340. http://dx.doi.org/10.1038/383337a0

Miller, C. 1982. Open-state substructure of single chloride channels from *Torpedo* electroplax. *Philos. Trans. R. Soc. Lond. B Biol. Sci.* 299:401–411. http://dx.doi.org/10.1098/rstb.1982.0140

Miller, C., and M.M. White. 1984. Dimeric structure of single chloride channels from *Torpedo* electroplax. *Proc. Natl. Acad. Sci. USA.* 81:2772–2775. http://dx.doi.org/10.1073/pnas.81.9.2772

Miyawaki, A., and R.Y. Tsien. 2000. Monitoring protein conformations and interactions by fluorescence resonance energy transfer between mutants of green fluorescent protein. *Methods Enzymol.* 327:472–500.

Nguitragool, W., and C. Miller. 2007. CLC Cl^-/H^+ transporters constrained by covalent cross-linking. *Proc. Natl. Acad. Sci. USA.* 104:20659–20665. http://dx.doi.org/10.1073/pnas.0708639104

Puljung, M.C., and W.N. Zagotta. 2011. Labeling of specific cysteines in proteins using reversible metal protection. *Biophys. J.* 100:2513–2521. http://dx.doi.org/10.1016/j.bpj.2011.03.063

Pusch, M., K. Steinmeyer, M.C. Koch, and T.J. Jentsch. 1995. Mutations in dominant human myotonia congenita drastically alter the voltage dependence of the CIC-1 chloride channel. *Neuron.* 15:1455–1463. http://dx.doi.org/10.1016/0896-6273(95)90023-3

Robertson, J.L., L. Kolmakova-Partensky, and C. Miller. 2010. Design, function and structure of a monomeric ClC transporter. *Nature.* 468:844–847. http://dx.doi.org/10.1038/nature09556

Rulíšek, L., and J. Vondrásek. 1998. Coordination geometries of selected transition metal ions (Co^{2+}, Ni^{2+}, Cu^{2+}, Zn^{2+}, Cd^{2+}, and Hg^{2+}) in metalloproteins. *J. Inorg. Biochem.* 71:115–127. http://dx.doi.org/10.1016/S0162-0134(98)10042-9

Rychkov, G.Y., D. St J. Astill, B. Bennetts, B.P. Hughes, A.H. Bretag, and M.L. Roberts. 1997. pH-dependent interactions of Cd^{2+} and a carboxylate blocker with the rat C1C-1 chloride channel and its R304E mutant in the Sf-9 insect cell line. *J. Physiol.* 501:355–362. http://dx.doi.org/10.1111/j.1469-7793.1997.355bn.x

Saviane, C., F. Conti, and M. Pusch. 1999. The muscle chloride channel ClC-1 has a double-barreled appearance that is differentially affected in dominant and recessive myotonia. *J. Gen. Physiol.* 113:457–468. http://dx.doi.org/10.1085/jgp.113.3.457

Stauber, T., S. Weinert, and T.J. Jentsch. 2012. Cell biology and physiology of CLC chloride channels and transporters. *Compr. Physiol.* 2:1701–1744.

Tseng, P.Y., B. Bennetts, and T.Y. Chen. 2007. Cytoplasmic ATP inhibition of CLC-1 is enhanced by low pH. *J. Gen. Physiol.* 130:217–221. http://dx.doi.org/10.1085/jgp.200709817

Yellen, G., D. Sodickson, T.Y. Chen, and M.E. Jurman. 1994. An engineered cysteine in the external mouth of a K^+ channel allows inactivation to be modulated by metal binding. *Biophys. J.* 66:1068–1075. http://dx.doi.org/10.1016/S0006-3495(94)80888-4

Zhang, X.D., and T.Y. Chen. 2009. Amphiphilic blockers punch through a mutant CLC-0 pore. *J. Gen. Physiol.* 133:59–68. http://dx.doi.org/10.1085/jgp.200810005

Zhang, X.D., Y. Li, W.P. Yu, and T.Y. Chen. 2006. Roles of K149, G352, and H401 in the channel functions of ClC-0: Testing the predictions from theoretical calculations. *J. Gen. Physiol.* 127:435–447. http://dx.doi.org/10.1085/jgp.200509460

Zhang, X.D., P.Y. Tseng, and T.Y. Chen. 2008. ATP inhibition of CLC-1 is controlled by oxidation and reduction. *J. Gen. Physiol.* 132:421–428. http://dx.doi.org/10.1085/jgp.200810023

Zhang, X.D., W.P. Yu, and T.Y. Chen. 2010. Accessibility of the CLC-0 pore to charged methanethiosulfonate reagents. *Biophys. J.* 98:377–385. http://dx.doi.org/10.1016/j.bpj.2009.09.066

Zheng, J., M.C. Trudeau, and W.N. Zagotta. 2002. Rod cyclic nucleotide-gated channels have a stoichiometry of three CNGA1 subunits and one CNGB1 subunit. *Neuron.* 36:891–896.

Zheng, J., M.D. Varnum, and W.N. Zagotta. 2003. Disruption of an intersubunit interaction underlies Ca^{2+}-calmodulin modulation of cyclic nucleotide-gated channels. *J. Neurosci.* 23:8167–8175.